Acta Crystallographica Section D
Biological Crystallography
ISSN 0907-4449

Surface-entropy reduction approaches to manipulate crystal forms of β-ketoacyl acyl carrier protein synthase II from *Streptococcus pneumoniae*

Gopalakrishnan Parthasarathy, Richard Cummings, Joseph W. Becker and Stephen M. Soisson*

Merck Research Laboratories, Rahway, NJ, USA

Correspondence e-mail: stephen_soisson@merck.com

Received 17 October 2007
Accepted 2 November 2007

PDB Reference: β-ketoacyl acyl carrier protein synthase II, 2rjt, r2rjtsf.

A series of experiments with β-ketoacyl acyl carrier protein synthase II (FabF) from *Streptococcus pneumonia* (spFabF) were undertaken to evaluate the capability of surface-entropy reduction (SER) to manipulate protein crystallization. Previous work has shown that this protein crystallizes in two forms. The triclinic form contains four molecules in the asymmetric unit (a.u.) and diffracts to 2.1 Å resolution, while the more desirable primitive orthorhombic form contains one molecule in the a.u. and diffracts to 1.3 Å. The aim was to evaluate the effect of SER mutations that were specifically engineered to avoid perturbing the crystal-packing interfaces employed by the favorable primitive orthorhombic crystal form while potentially disrupting a surface of the protein employed by the less desirable triclinic crystal form. Two mutant proteins were engineered, each of which harbored five SER mutations. Extensive crystallization screening produced crystals of the two mutants, but only under conditions that differed from those used for the native protein. One of the mutant proteins yielded crystals that were of a new form (centered orthorhombic), despite the fact that the interfaces employed by the primitive orthorhombic form of the native protein were specifically unaltered. Structure determination at 1.75 Å resolution reveals that one of the mutations, E383A, appears to play a key role in disfavouring the less desirable triclinic crystal form and in generating a new surface for a packing interaction that stabilizes the new crystal form.

1. Introduction

The preparation of high-quality crystals for use in X-ray diffraction experiments is a significant rate-limiting step in the process of macromolecular structure determination. It follows that crystallization continues to be the major barrier to successful project completion in the traditional academic setting, high-throughput genomics endeavors and pharmaceutical drug discovery. The situation can appear to be particularly hopeless when one considers the intrinsically low success rate of protein crystallization in general (Hui & Edwards, 2003). For these reasons, protein crystallographers are extremely interested in techniques that expand the sphere of proteins amenable to crystallization, increase the probability of success and have the potential to manipulate specific crystallization properties such as space groups.

Surface-entropy reduction (SER) is one of the most exciting new techniques to address the relatively low probability of success in protein crystallization (Cooper *et al.*, 2007; Derewenda, 2004; Goldschmidt *et al.*, 2007). The pioneering work of Derewenda and colleagues has shown that mutation of surface residues with large conformational flexibility to

smaller side chains with less intrinsic entropy can often result in mutant proteins that crystallize under more conditions and often diffract to higher resolution than their native counterparts (Derewenda, 2004). For example, early studies with the RhoGDI protein showed that targeting clusters of Lys or Glu residues and mutating them to Ala significantly improved the crystallization properties of the protein, which in its native state was difficult to crystallize (Longenecker *et al.*, 2001; Mateja *et al.*, 2002). Furthermore, a double mutant of RhoGDI resulted in crystals in which the native diffraction limit was improved from 2.5 to 1.25 Å (Mateja *et al.*, 2002). Significant work has also been performed to show the value of using other replacement residues such as His, Ser, Thr, Tyr (Cooper *et al.*, 2007) and Arg (Czepas *et al.*, 2004) in addition to Ala. The SER approach has been expanded and refined over the past 15 y to the point where an online server now exists that will suggest optimal sites for SER based on sequence analysis (Goldschmidt *et al.*, 2007).

In the course of our own internal evaluation of the SER approach as it relates to the problems typically encountered in industrial crystallography, we were interested in testing the power of the technique in the context of a known system. We chose the β-ketoacyl acyl carrier protein synthase II (FabF) from *Streptococcus pneumoniae* as our test protein. FabF belongs to the KASII family of enzymes that catalyze the essential two-carbon addition chain-elongation step of fatty-acid synthesis in bacteria (Lai & Cronan, 2003; Revill *et al.*, 2001; Schujman *et al.*, 2001; Tsay *et al.*, 1992) and are of pharmaceutical importance as the target of platensimycin, a potent antibiotic (Wang *et al.*, 2006). Structural studies of the FabF protein from *S. pneumoniae* (spFabF) revealed that the native protein crystallizes in two forms (Price *et al.*, 2003). The triclinic crystal form contains four molecules in the asymmetric unit (a.u.) and diffracts X-rays to 2.1 Å resolution. An alternative, primitive orthorhombic crystal form also exists which is somewhat preferable because it only has one molecule in the a.u. and diffracts X-rays to 1.3 Å resolution. We wished to find out what would happen if one were to start with a protein that was known to form high-resolution crystals and design a set of SER mutations that specifically avoided the known crystal contacts that were involved in the high-resolution crystal form. Knowing that the native protein has the capability of forming a high-resolution crystal form, what effect would targeted SER mutations have on the physical properties of the protein and its ability to crystallize? As an additional motivation for this study, we were concerned that the binding of various ligands to the wild-type spFabF protein might render the protein less amenable to crystallization and we hoped to generate a repertoire of spFabF proteins with different crystallization properties that could be used to potentially overcome these difficulties.

We designed two mutant forms of spFabF in which five hand-selected Glu and Lys residues were mutated to Ala. The first mutant (M1) has five nonclustered Glu-Ala mutations that were chosen to specifically preserve crystal contacts in the favoured primitive orthorhombic crystal form. For the second mutant (M2), we kept the five targeted residues limited to two tight clusters identified on the surface, again avoiding sites that are directly involved in or are in close proximity to the packing interfaces used to form the high-resolution primitive orthorhombic crystal form. An analysis of the resultant M1 crystal structure shows that one of the five residue positions mutated (E383A) appears to play a critical role in driving the formation of a new crystal form with this variant by facilitating the formation of a new packing interface between two dyad symmetry-related molecules. This study highlights the considerable power of the SER approach for creating new crystal-packing interfaces that result in new crystal forms of proteins diffracting to high resolution.

2. Materials and methods

2.1. Cloning

The putative *fabF* gene, encoding a β-ketoacyl acyl carrier protein synthase II (FabF) homologue (AF197933), was PCR-amplified from *S. pneumoniae* chromosomal DNA using the forward primer 5′-**CATATG**AAACTAAATCGAGTAG-3′ and the reverse primer 5′-**CTCGAG**TTACGCCCAACGTT-TGA-3′ and cloned into TA vector (Invitrogen Inc., Carlsbad, California, USA). The forward primer 5′–3′ was designed to introduce an *Nde*I restriction site (bold) and the reverse primer 5′–3′ was designed to introduce a stop codon and an *Xho*I (bold) restriction site downstream of the *FabF* gene. Two mutant proteins were designed and generated: mutant 1 (M1), spFabF(1–409) E22A, E94A, E325A, E383A, E409A, and mutant 2 (M2), spFabF(1–411) E244A, E247A, K248A, E383A, E385A.

M1 was generated using five iterative cycles of single-point mutation using the QuikChange site-directed mutagenesis kit (Stratagene Inc., La Jolla, California, USA) and M2 was generated using two cycles of cluster mutations on the TA clone. The *fabF* gene was then excised using *Nde*I and *Xho*I restriction enzymes and ligated in-frame into the *Nde*I/*Xho*I-digested pET-15b expression vector with an N-terminal His tag (Novagen Inc., Madison, Wisconsin, USA) to construct plasmids pXspFabF(M1) and pXspFabF(M2). The resulting plasmids were transformed into *Escherichia coli* XL1-Blue competent cells and the clones were sequence-verified for any random mutations. Subsequently, pXSpFabF(M1) and pXspFabF(M2) isolated from *E. coli* XL1-Blue cells were transformed into the expression strain *E. coli* BL21 (DE3).

2.2. Protein expression and purification

Identical protein-expression and purification procedures were used for both the M1 and M2 variants of spFabF. Transformed cells were grown on Luria–Bertani (LB) agar plates supplemented with ampicillin (100 μg ml^{-1}). SDS–PAGE analysis was used to screen colonies for overexpression of spFabF(M1). One such positive colony was used to inoculate 100 ml LB medium with 100 μg ml^{-1} ampicillin and grown overnight at 310 K. Fresh LB medium (5 l) was inoculated with the overnight cultures and grown at 310 K until the OD_{600} reached 0.7. FabF expression was induced with 1 m*M* IPTG

for 18 h at 291 K and cells were harvested by centrifugation (6000*g*, 15 min at 277 K), washed twice with phosphate-buffered saline and the pellet was frozen at 193 K. For purification, the frozen pellets were resuspended in cold lysis buffer (20 m*M* Tris–HCl pH 8.0, 10% glycerol, 500 m*M* NaCl, 20 m*M* imidazole, 2.5 m*M* β-mercaptoethanol) and lysed by three passes through an Avestin Emulsiflex C-5 high-pressure homogenizer (Avestin Inc., Ottawa, Ontario, Canada). The crude lysate was clarified by centrifugation at 60 000*g* for 45 min at 277 K. The clarified cell extract was then applied onto a 25 ml Ni–NTA affinity column (Qiagen Inc., Chatsworth, California, USA) that had been pre-equilibrated with the lysis buffer. The column was then washed with 100 ml lysis buffer followed by a 50 ml step gradient of lysis buffer containing 300 m*M* imidazole and a 50 ml wash with 1 *M* imidazole in lysis buffer. The FabF-containing fractions (50 ml) were pooled and dialysed overnight against 4 l of buffer containing 20 m*M* Tris–HCl pH 8.0, 50 m*M* NaCl, 10% glycerol, 1 m*M* DTT at 277 K. The dialysed sample was then loaded onto a MonoQ ion-exchange column (GE Healthcare, Piscataway, New Jersey, USA) and washed with buffer *A* (20 m*M* Tris–HCl pH 8.0, 50 m*M* NaCl, 1 m*M* DTT) followed by a two column-volume linear gradient from 0 to 1 *M* NaCl in buffer *A*. The spFabF-containing fractions were pooled, concentrated and loaded onto a Superdex 75 gel-filtration column (GE Healthcare, Piscataway, New Jersey, USA). The final elution buffer was 20 m*M* Tris–HCl pH 8.0, 50 m*M* NaCl, 10% glycerol, 1 m*M* DTT. The pooled fractions were concentrated to 30 mg ml^{-1} and flash-frozen in liquid nitrogen for use in crystallization and ligand-binding studies. At each stage of purification, SDS–PAGE analysis with Coomassie Blue stain was used to identify FabF-containing fractions.

2.3. Crystallization

Both proteins (M1 and M2) were screened for crystallization using Crystal Screens I and II and Index Screen (Hampton Research, Aliso Viejo, California, USA). The screens were performed in a Q Plate II (Hampton Research) using the hanging-drop vapour-diffusion method at room temperature. Each hanging droplet on the siliconized cover slip consisted of 1 µl protein solution at 10 mg ml^{-1} (buffer: 20 m*M* Tris–HCl pH 8.0, 50 m*M* NaCl, 10% glycerol) and 1 µl precipitating solution. The reservoir contained 0.5 ml of the same precipitant. *De novo* microcrystals of spFabF(M1) and spFabF(M2) grew under a number of conditions from the Index Screen and Crystal Screens I and II. The most promising conditions for both proteins were optimized.

2.4. Data collection and structure determination

All data were collected under cryogenic conditions (100 K) in the facilities of the Industrial Macromolecular Crystallography Association Collaborative Access Team (IMCA-CAT) at the Advanced Photon Source (Argonne National Laboratory, Argonne, Illinois, USA). Before freezing, the crystals were cryoprotected by sequential immersion in reservoir solution supplemented with 12.5% and 15% ethylene glycol. All crystals were flash-frozen in liquid nitrogen prior to data collection. Data were integrated and scaled using the *HKL*-2000 program suite (Otwinowski & Minor, 1997). The crystal structure of the M1 protein was determined using standard molecular-replacement techniques *via* the *MOLREP* program (Vagin & Teplyakov, 2000; Vagin & Isupov, 2001) using the structure of wild-type spFabF (PDB code 1ox0) as a search model. The structure was manually rebuilt using *O* (Jones *et*

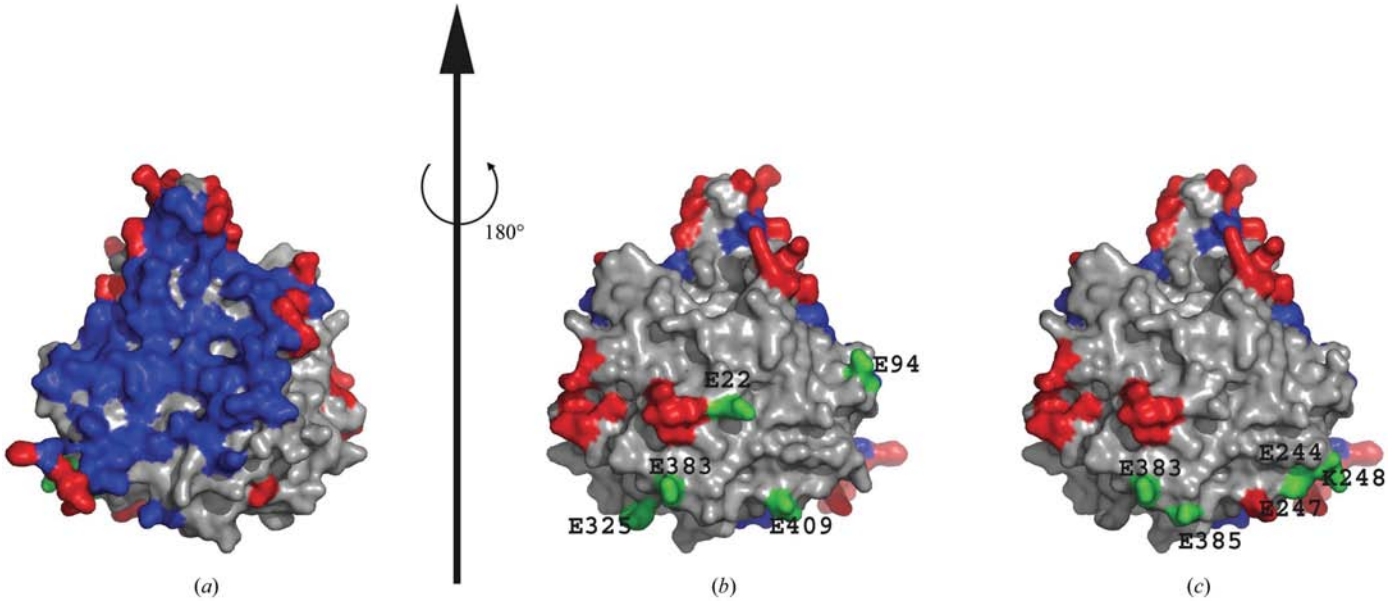

Figure 1
Design of the M1 and M2 spFabF variant proteins. The surface of the spFabF monomer from the primitive orthorhombic crystal form (PDB code 1ox0) is depicted and coloured to show residues involved in dimer-interface contacts (blue), crystal-packing contacts (red) and sites targeted for SER mutation (green). (*a*) Side view of the protein, showing mostly the dimer interface. (*b*) Opposite side of the protein, showing residues chosen for SER mutations in the M1 protein (green). (*c*) Similar view to (*b*), but with residues targeted in the M2 protein shown in green.

al., 1991) followed by iterative rounds of refinement and water placement using *autoBUSTER* (Roversi *et al.*, 2000). Surface-area calculations were performed using *AREAIMOL* and structural alignments and r.m.s.d. calculations were performed using *LSQKAB* as implemented in the *CCP*4 suite of programs (Collaborative Computational Project, Number 4, 1994). Molecular graphics images were prepared using *PyMOL* (DeLano, 2002) and standard graphics-editing programs.

3. Results

3.1. Mutant design, construction and purification

In order to evaluate the effects of a targeted SER approach using the spFabF protein, we decided to focus on Glu and Lys residues on the surface of the protein, based on earlier successes reported in the literature (Longenecker *et al.*, 2001; Mateja *et al.*, 2002). An examination of the primary sequence and crystal structure of spFabF (PDB code 1ox0) showed that there are 22 Lys and 30 Glu residues present in the portion of spFabF visible in the high-resolution crystal structure. Since the biologically active form of the protein is a homodimer, it seemed prudent to exclude residues that are close to or involved in forming the dimer interface (Fig. 1*a*). Bearing that constraint in mind, two mutant proteins were designed.

The first mutant protein, M1, was designed after careful inspection of the packing interactions utilized by the protein in the published high-resolution primitive orthorhombic crystal form. Five Glu residues that do not appear to make interactions with symmetry-related molecules in the primitive orthorhombic crystal lattice were chosen for SER mutation to Ala. These residues are Glu22, Glu94, Glu325, Glu383 and Glu409 (Fig. 1*b*). The last residue, Glu409, is at the C-terminus of the M1 protein. The backbone atoms of this residue are within 4 Å of a symmetry-related molecule and a very small patch of crystal contact surface (Fig. 1*b*); however, the side chain appears to be completely independent of this small contact and was judged to be safe for mutagenesis.

A second mutant, M2, was designed to further test the effect of targeted SER mutations that avoid known crystal contacts. For the M2 protein, we targeted clusters of Glu and Lys residues on the protein (Fig. 1*c*). As has been pointed out previously, restricting the mutagenesis to clusters of residues is advantageous in the case of designing SER mutations based solely on primary sequence information since clusters of charged residues are almost always found on the surface (Baud & Karlin, 1999). It is also a convenient approach owing to the fact that multiple mutations can be made during one PCR-based mutagenesis experiment. The five residues targeted for M2 fall into two clusters. Cluster one consists of residues Glu244, Glu247 and Lys248, while cluster two is comprised of residues Glu383 and Glu385 (Fig. 1*c*).

It should also be noted that one of the side chains targeted in both the M1 and M2 proteins, Glu383, is part of a large crystal-packing interface in the less favourable triclinic crystal form of native spFabF (PDB code 1oxh; Figs. 2*a* and 2*b*). Two of the four molecules present in the a.u. of the triclinic crystals pack in exactly the same manner, situating the Glu383 side chain in a crevice on a symmetry-related molecule (Fig. 2*b*) where it is within 4 Å of four residues (Asn69, Lys131, Met133 and Lys137). Although it is debatable whether such an interaction is energetically favorable (Derewenda & Vekilov, 2006), we speculate that the presence of potential salt-bridge

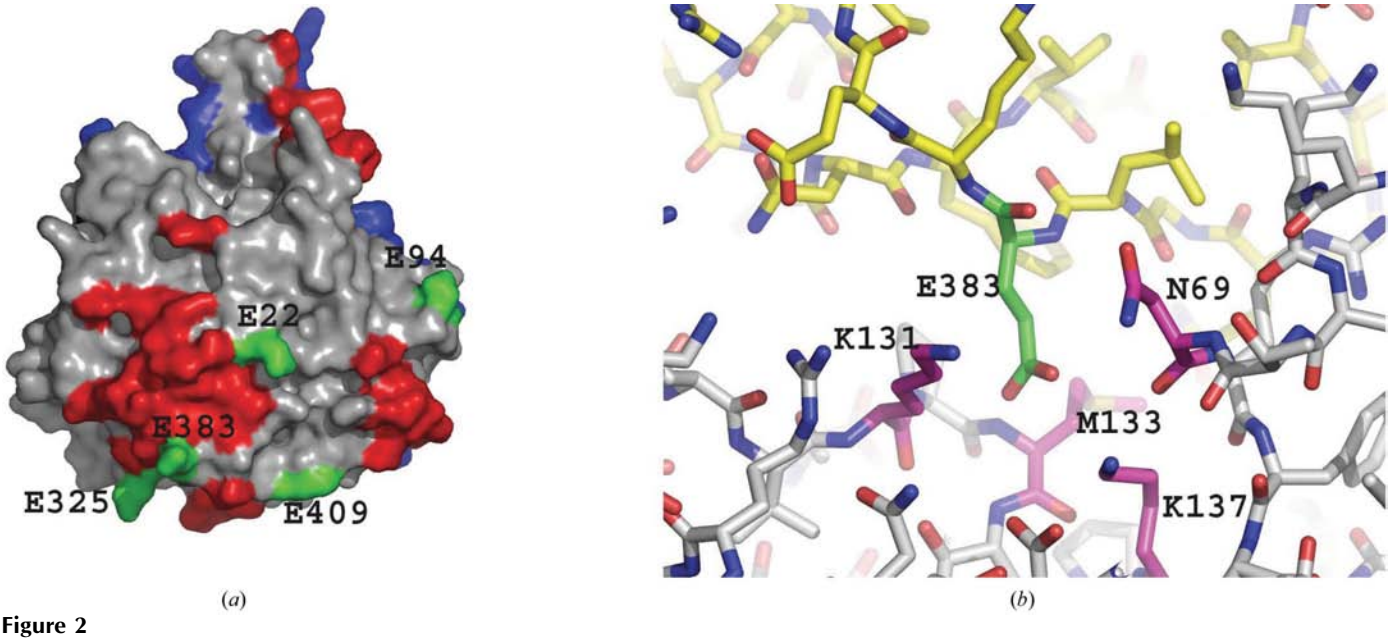

Figure 2
Native spFabF triclinic packing interface. (*a*) The surface of the spFabF monomer (chain *A*) present in the triclinic crystal form (PDB code 1oxh) is depicted and coloured to show the residues involved in dimer-interface contacts (blue), crystal-packing contacts (red) and sites targeted for SER mutations in protein M1 (green). (*b*) Close-up view of the triclinic crystal-packing interaction, with Glu383 in green and the residues discussed in the text shown in magenta.

interactions and a large van der Waals contact surface would make this an energetically neutral or perhaps slightly favourable interaction. It therefore remains a formal possibility that the E383A mutation has the additional benefit of being disruptive of the P1 packing interaction and would lead to preferential crystallization in the superior orthorhombic crystal setting. The cloning of the spFabF gene and subsequent site-directed mutagenesis were performed as described in §2. Each mutation was sequence-verified and the two mutant proteins were subcloned into pET-15b expression vectors to generate the final N-terminally His-tagged expression vector constructs.

Both spFabF mutant proteins were purified using metal-chelate affinity chromatography, ion-exchange and size-exclusion chromatography, with an overall yield of approximately 20 mg per litre of culture for both the spFabF(M1) and spFabF(M2) proteins. We have been able to concentrate the proteins to 50 mg ml^{-1} without precipitation or aggregation. The high expression level and ability to significantly concentrate both proteins suggests that the designed mutations do not affect the folding and the solubility of the protein. The purified spFabF(M1) and spFabF(M2) proteins appeared as homogeneous bands on SDS–PAGE that migrated in positions consistent with the calculated molecular weights of 45 400 and 45 782 Da, respectively. By LC–MS, the molecular weights of the purified proteins were determined to be 45 392 and 45 778 Da respectively, in excellent agreement with the predicted weights of the proteins based on the FabF sequence including the polyhistidine tag and thrombin cleavage site. The mutant proteins also retained the ability to tightly bind platensimycin (data not shown) using a previously described direct binding assay (Wang *et al.*, 2006), bolstering the case that the mutations have no adverse functional consequences on the enzyme.

3.2. Crystallization screening and optimization

For crystallographic studies, purified spFabF was diluted to 10 mg ml^{-1} in buffer containing 20 m*M* Tris–HCl pH 8.0, 1 m*M* DTT, 50 m*M* NaCl and 10% glycerol. Initial attempts to reproduce the published crystallization conditions for the native protein using our mutant variants only yielded amorphous precipitates that we were not able to improve. We then subjected the M1 and M2 proteins to a standard battery of broad crystallization screens that yielded microcrystals in a number of different conditions.

The most promising crystallization condition for M1 (0.2 *M* ammonium acetate, 0.1 *M* MES pH 6.5, 20% PEG 3350) was further optimized by varying the precipitant concentration, pH and salt concentration. After several attempts to slow nucleation and reduce background precipitation, we observed that the addition of 10% ethylene glycol to the reservoir solution resulted in a clear background with fewer needles and some amorphous spherical crystals. More extensive additive screening identified 1% benzamidine–HCl as an additive that converted the initial needles into small blocky crystals. Subsequent optimization using microseeding techniques (5–12% PEG 3350, 0.1 *M* MES pH 6.5, 1% benzamidine–HCl, 10% ethylene glycol, 1 m*M* DTT) yielded diffraction-quality crystals.

The optimization of M2 crystals proved more challenging, despite the fact that the initial conditions (0.2 *M* sodium acetate, 0.1 *M* Tris–HCl pH 8.5, 30% PEG 4000) were very promising. The *de novo* crystals grew as large clusters; however, extensive crystallization screens, additive screens and microseeding approaches failed to yield crystals that were suitable for diffraction analysis.

Table 1
X-ray data and refinement statistics.

Values in parentheses are for the highest resolution shell.

Space group	$C222_1$
Unit-cell parameters (Å)	a = 112.42, b = 115.87, c = 278.92
$d_{\rm min}$ (Å)	1.75
No. of observations	1955728
No. of unique observations	181565
Completeness (%)	99.6 (97.9)
$I/\sigma(I)$	13.8
$R_{\rm merge}$† (%)	5.9 (47.5)
Resolution range (Å)	140–1.75
R factor (%)	16.9
$R_{\rm free}$‡ (%)	20.6
Protein atoms	12210
Solvent molecules	1791
R.m.s.d. bonds (Å)	0.011
R.m.s.d. angles (°)	1.332

† $R_{\rm merge} = \sum_{hkl}\sum_i |I_i(hkl) - \overline{I(hkl)}|/\sum_{hkl}\sum_i I_i(hkl)$, where $I_i(hkl)$ is the integrated intensity for a given reflection. ‡ $R_{\rm free}$ is calculated as the conventional crystallographic R factor but using a randomly selected 5% subset of reflections not included in the refinement process.

3.3. Structure determination and analysis

Crystals of the spFabF(M1) protein were analyzed using synchrotron radiation at the IMCA beamline at the Advanced Photon Source. The crystals form in space group $C222_1$, with

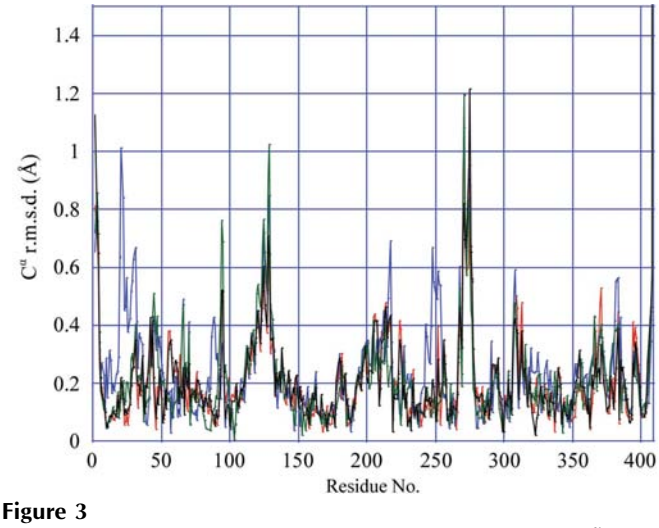

Figure 3
R.m.s. deviation of the M1 structure compared with 1ox0. The C^{α} r.m.s.d. (Å) between each of the four monomers in the a.u. of the M1 crystals and the monomer from 1ox0 is shown. Monomer *A* is in red, monomer *B* blue, monomer *C* green and monomer *D* black.

unit-cell parameters a = 112.42, b = 115.87, c = 278.92 Å, and contain four molecules in the a.u. This crystal form differs from both crystal forms observed with the native protein. The native protein's primitive orthorhombic unit-cell parameters were a = 63.7, b = 90.0, c = 62.2 Å with one molecule in the a.u. and the triclinic parameters were a = 61.5, b = 71.6, c = 96.1 Å, α = 89.9, β = 83.1, γ = 69.1° with four molecules in the a.u. (Price *et al.*, 2003). The structure of spFabF(M1) was determined using standard molecular-replacement techniques utilizing the wild-type structure of spFabF (PDB code 1ox0) as a search model. The initial electron-density maps were of very high quality and confirmed the presence of the expected SER mutations; the final refined structure at 1.75 Å resolution is of very high quality. Data-collection and structure-refinement statistics are summarized in Table 1. Since the structure of spFabF has been described in detail elsewhere (Price *et al.*, 2003), as have many other members of the KASII family of condensing enzymes (Huang *et al.*, 1998; McGuire *et al.*, 2001; Moche *et al.*, 2001; Olsen *et al.*, 1999; Price *et al.*, 2001; Wang *et al.*, 2006), it would be redundant to elaborate on the structure here. Briefly, the KASII enzymes share the mixed α–β fold of the thiolase family of enzymes (Mathieu *et al.*, 1997) and function as homodimeric assemblies of 45 kDa monomers. The M1 structure superimposes on the native spFabF structure with an average C^{α} r.m.s.d. of 0.224 Å and there appears to be no significant distortion of the protein structure as a result of the five SER mutations (Fig. 3). Areas of the protein with the highest r.m.s. deviation from the native structure (PDB code 1ox0) are confined to loop and surface residues that might be expected to have intrinsically high relative mobility. A minor difference observed in the M1 structure is the absence of a magnesium ion previously observed near a conserved buried charge pair as discussed previously (Price *et al.*, 2003). In the current M1 structure, the crystals were grown in the absence of magnesium and the corresponding site is occupied by a water molecule (not shown). Since this magnesium ion was shown to be non-essential for spFabF functionality (Price *et al.*, 2003), it seems reasonable that the water molecule observed in this structure is relevant. Interestingly, we tested the effect of magnesium salts as additives in the crystallization screening and optimization for the M1 and M2 proteins; however, inclusion of magnesium consistently inhibited crystallization of these variant proteins.

3.4. New interface formed by the E383A mutation

The mutation of Glu383 to Ala in the M1 protein results in the formation of a new packing interface on the surface of the protein. It is interesting that Glu383 and residues in its vicinity are not used in the primitive orthorhombic form of the native crystals (Fig. 1); however, the side chain of Glu383 is part of a different large interface that is exploited by the triclinic crystal form (Fig. 2). Although the surface of the protein utilized in the triclinic form spatially overlaps with the surface of the protein used to facilitate formation of the new crystal form that results from the E383A mutation, the packing occurs in a very different manner (Fig. 4). The new interface is formed between two dyad symmetry-related molecules centered at the E383A mutation (Figs. 4 and 5). The CB atoms from each E383A residue are at a van der Waals contact distance from the CA atom of the flanking residue, Lys384, in the symmetry-related molecule. The newly formed interface buries approximately 665 $Å^2$ of surface area on each of the two molecules and consists of direct interactions between E383A from both monomers, as well as spatially adjacent residues such as Phe358 (Fig. 5). It seems clear that the new interface could not form with the native Glu residue at position 383 owing to steric clashes and that the E383A mutation is directly responsible for the formation of the new interaction.

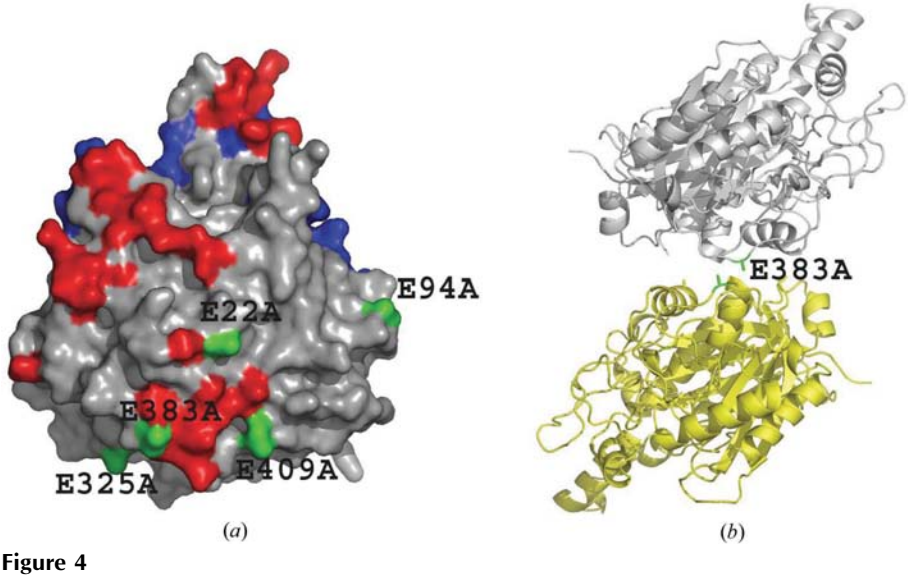

Figure 4
M1 packing surface and new packing interaction. (*a*) The M1 protein surface (chain *A*) coloured as in Figs. 1 and 2, highlighting the sites of the M1 mutations (green). (*b*) Overall ribbon structure of two monomers involved in making the new crystal-packing interaction observed in the structure.

4. Conclusions and discussion

In summary, we have evaluated the effects of SER mutations on the spFabF protein that were rationally designed to avoid the disruption of interfaces involved in the formation of a high-resolution (1.3 Å) crystal form while at the same time potentially destabilizing a less desirable triclinic crystal form. It was our expectation that the mutant proteins would crystallize in the same space group as the native protein since we carefully avoided altering the presumably strong interfaces that are used in this well diffracting crystal form. Interestingly, the M1 protein was observed to crystallize preferentially in yet another new crystal form, despite our efforts to preserve these crystal interfaces.

We observed that the new centered orthorhombic crystal form is held together by a new lattice contact that occurs between dyad symmetry-related molecules at the site of one of the SER mutations, E383A. Interestingly, this Glu side chain does not participate in lattice interactions in the native primitive orthorhombic crystal form; however, Glu383 does mediate an important interaction that leads to formation of the triclinic crystals. These results suggest the E383A mutation plays a critical role in both disfavouring the less desirable triclinic form and also in generating a new surface on the protein that is a driving force in the formation of the new centered orthorhombic crystal lattice. The preponderance of interactions observed in the new interface are between backbone atoms and/or immobilized hydrophobic residues, which is consistent with the hypothesis set forward by Derewenda and colleagues (Derewenda, 2004; Derewenda & Vekilov, 2006; Longenecker *et al.*, 2001) that reducing surface entropy can favour crystallization by reducing the free-energy cost of forming a packing interface.

It is curious that despite our efforts to preserve known crystal contacts that lead to well diffracting crystals, the mutant protein crystallizes in an entirely different space group. This observation makes it tempting to conclude that the newly created interface resulting from the E383A mutation is strong enough in effect to form preferentially over the original lattice contacts. This conclusion is tempered by the unfortunate reality that the driving forces of crystallization are poorly understood, especially considering that the mutant protein described in this paper bears multiple charge-to-neutral mutations that must alter the isoelectric point and solution properties of the protein. Our results are consistent with an earlier observation that new crystal lattices formed by SER mutant proteins are predominantly held together by the sites of mutation through homotypic interactions (Longenecker *et al.*, 2001). This remarkable fact is overwhelmingly supported by the results presented here and serves to highlight the hypothesis that surfaces of proteins have carefully evolved to minimize serendipitous protein–protein interactions (Doye *et al.*, 2004). Further support of this hypothesis comes from the numerous studies showing the power of the SER approach in increasing the probability and scope of protein crystallization (Cooper *et al.*, 2007; Czepas *et al.*, 2004; Longenecker *et al.*, 2001; Mateja *et al.*, 2002). Clearly, these repeated observations, made in the context of many different proteins, show that simple changes on the surface of a protein can often lead to productive protein–protein interactions.

There is still much work to be done in designing SER mutations that increase the probability of success. For instance, the work presented here broadly shows two distinct approaches to mutant design. One mutant has a dispersed set of mutations and the other has two small clusters of residues, yet only the first mutant yielded usable crystals. The recent work in expanding the repertoire of the SER toolkit (Cooper *et al.*, 2007), as well as the construction of an automated procedure for mutant design (Goldschmidt *et al.*, 2007), lends confidence that SER will play an increasingly important role as protein crystallography expands to new and more complex targets.

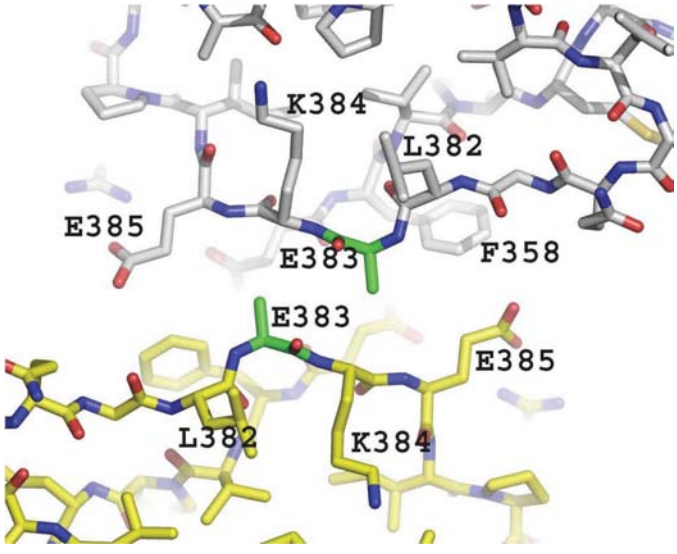

Figure 5
Close-up view of new packing interface, showing the interactions at the new interface formed between two symmetry-related molecules (yellow and grey). The E383A mutation is highlighted in green.

We thank the staff of the IMCA-CAT beamlines at the Advanced Photon Source (Argonne, Illinois, USA) for help with data collection. Use of the IMCA-CAT beamlines at the APS was supported by the companies of the Industrial Macromolecular Crystallography Association through a contract with the Center for Advanced Radiation Sources at the University of Chicago. We would also like to thank S. B. Singh, J. Wang, J. Heck and D. Cully for encouragement, advice and support.

References

Baud, F. & Karlin, S. (1999). *Proc. Natl Acad. Sci. USA*, **96**, 12494–12499.
Collaborative Computational Project, Number 4 (1994). *Acta Cryst.* D**50**, 760–763.
Cooper, D. R., Boczek, T., Grelewska, K., Pinkowska, M., Sikorska, M., Zawadzki, M. & Derewenda, Z. (2007). *Acta Cryst.* D**63**, 636–645.
Czepas, J., Devedjiev, Y., Krowarsch, D., Derewenda, U., Otlewski, J. & Derewenda, Z. S. (2004). *Acta Cryst.* D**60**, 275–280.
DeLano, W. L. (2002). *The PyMOL Molecular Graphics System.* http://www.pymol.org.
Derewenda, Z. S. (2004). *Structure*, **12**, 529–535.
Derewenda, Z. S. & Vekilov, P. G. (2006). *Acta Cryst.* D**62**, 116–124.
Doye, J. P., Louis, A. A. & Vendruscolo, M. (2004). *Phys. Biol.* **1**, P9–P13.
Goldschmidt, L., Cooper, D. R., Derewenda, Z. S. & Eisenberg, D. (2007). *Protein Sci.* **16**, 1569–1576.
Huang, W., Jia, J., Edwards, P., Dehesh, K., Schneider, G. & Lindqvist, Y. (1998). *EMBO J.* **17**, 1183–1191.
Hui, R. & Edwards, A. (2003). *J. Struct. Biol.* **142**, 154–161.
Jones, T. A., Zou, J.-Y., Cowan, S. W. & Kjeldgaard, M. (1991). *Acta Cryst.* A**47**, 110–119.
Lai, C.-Y. & Cronan, J. E. (2003). *J. Biol. Chem.* **278**, 51494–51503.
Longenecker, K. L., Garrard, S. M., Sheffield, P. J. & Derewenda, Z. S. (2001). *Acta Cryst.* D**57**, 679–688.

McGuire, K. A., Siggaard-Andersen, M., Bangera, M. G., Olsen, J. G. & von Wettstein-Knowles, P. (2001). *Biochemistry*, **40**, 9836–9845.
Mateja, A., Devedjiev, Y., Krowarsch, D., Longenecker, K., Dauter, Z., Otlewski, J. & Derewenda, Z. S. (2002). *Acta Cryst.* D**58**, 1983–1991.
Mathieu, M., Modis, Y., Zeelen, J. P., Engel, C. K., Abagyan, R. A., Ahlberg, A., Rasmussen, B., Lamzin, V. S., Kunau, W. H. & Wierenga, R. K. (1997). *J. Mol. Biol.* **273**, 714–728.
Moche, M., Dehesh, K., Edwards, P. & Lindqvist, Y. (2001). *J. Mol. Biol.* **305**, 491–503.
Olsen, J. G., Kadziola, A., von Wettstein-Knowles, P., Siggaard-Andersen, M., Lindquist, Y. & Larsen, S. (1999). *FEBS Lett.* **460**, 46–52.
Otwinowski, Z. & Minor, W. (1997). *Methods Enzymol.* **276**, 307–326.
Price, A. C., Choi, K. H., Heath, R. J., Li, Z., White, S. W. & Rock, C. O. (2001). *J. Biol. Chem.* **276**, 6551–6559.
Price, A. C., Rock, C. O. & White, S. W. (2003). *J. Bacteriol.* **185**, 4136–4143.
Revill, W. P., Bibb, M. J., Scheu, A. K., Kieser, H. J. & Hopwood, D. A. (2001). *J. Bacteriol.* **183**, 3526–3530.
Roversi, P., Blanc, E., Vonrhein, C., Evans, G. & Bricogne, G. (2000). *Acta Cryst.* D**56**, 1316–1323.
Schujman, G. E., Choi, K. H., Altabe, S., Rock, C. O. & de Mendoza, D. (2001). *J. Bacteriol.* **183**, 3032–3040.
Tsay, J., Rock, C. & Jackowski, S. (1992). *J. Bacteriol.* **174**, 508–513.
Vagin, A. A. & Isupov, M. N. (2001). *Acta Cryst.* D**57**, 1451–1456.
Vagin, A. & Teplyakov, A. (2000). *Acta Cryst.* D**56**, 1622–1624.
Wang, J. *et al.* (2006). *Nature (London)*, **441**, 358–361.